# Recovery of Waste Farm After Methanation by Evaporation on Inclined Plate


**Hiba Zouaghi, Souad Harmand, and Sadok Ben Jabrallah**

## 1 Introduction

Wastes present problem for the entire population because of the nuisance it causes. In rural communities, it is rather animal waste, which causes a big problem (soil pollution, rivers, water table, etc.). These releases have a product rich in nutrients and fertilizers (Granier and Texier 1993). On this basis, several farmers choose recovery of such wastes by anaerobic digestion. The development of biogas plants not only reduces agricultural emissions by converting biomass but also thermal energy. This thermal energy can have other uses.

After anaerobic digestion, it leads to the production of two types of energy. One is related to the production of electricity and the other is reused in methanation process. The problem is that digestate, which causes, after anaerobic digestion, a problem on many levels. It has a high water content (up to 97%), particularly pig manure. That's why a storage or reuse is required. This product is the material remaining residue at the end of the process. It has excellent agronomic value and can be used as fertilizer (Latimier et al. 1996; Levasseur 1998).

The field of waste recovery appeared since a long time, especially in regard to farm waste, because of organic matter and fertilizers. Drying presents an important process for the management of farm waste, as it reduces mass and volume of the

H. Zouaghi (✉)
National Engineering School of Monastir, Avenue Ibn El Jazzar, Monastir 5019, Tunisia
e-mail: hibazouaghi@yahoo.fr

S. Harmand
University of Lille Nord, UVHC, LAMIH UMR CNRS 8201, Mont Houy, Valenciennes, Cedex 09 59300, France

S.B. Jabrallah
Sciences Faculty of Bizerte, Zarzouna, Bizerte 7021, Tunisia



F. Aloui, I. Dincer (eds.), *Exergy for A Better Environment and Improved Sustainability 1*, Green Energy and Technology,
https://doi.org/10.1007/978-3-319-62572-0_42

product and therefore cost of storage, workforce, and transportation. It's a method based on evaporation. This process, which is a change of vapor liquid phase, can be achieved by exposure to air. But, it can be intensified by the use of solar energy. This is one of the most practical of preserving the quality of agricultural products and recycling of waste and effluents methods. Studies on drying after anaerobic digestate are rare. However, other waste streams drying exist.

Drying is an important process for the management of sewage sludge, as it can reduce weight and volume of the product and therefore cost of storage, handling, and transportation. Solar drying plant of sewage sludge treatment was built as a tunnel-type greenhouse with a ceiling height of 2.5 m in Turkey (Salihoglu et al. 2006). It has been completely covered by two walls, with a thickness of 10 mm of transparent polycarbonate with light-transmitting sheet of 80%. Solar dryer was constructed with the principle of increasing the difference between vapor pressure of sludge compared to interior and relative vapor pressure to obtain an effective drying. Lei et al. (2009) developed a greenhouse solar dryer in China for drying sludge from wastewater treatment. The greenhouse is made of glass. Its inner lower surface is painted black in order to increase the absorption of solar radiation. A high stack of 180 cm was placed on top of the greenhouse. Samples of fresh sludge were obtained from wastewater treatment plant located in Shanghai. Initial slurry humidity is 5.16 kg/kg dry and dried at 0.78 kg/kg dry. It was rolled to 25 mm in thickness in a plate which was made from 0.1 mm steel mesh and a surface area of 0.22 m $\times$ 0.36 m. The drying process lasts 125 h in summer and about 550 h in winter with a non-regular decrease in moisture content (Bennamoun 2011).

Tannery effluent, ejected at environment, pollutes terrestrial and aquatic organisms in and around tanneries and evaporates over long periods. Drying may be accomplished by allowing effluent to flow on an inclined plane solar sensor. While liquid flows over collector, it is heated by solar energy that will help the increase of evaporation rate. In tannery, water effluent evaporation and recovery of salt is one of methods using solar energy available in abundance (Mani and Srinivasa Murthy 1993, 1994; Srithar and Mani 2003, 2004, 2006) used driers having sensor solar plates and a spray system to increase evaporation flow. In the case of plate sensor, effluent flows over the manifold. Therefore, effluent temperature at exposure area with air increases, which increases the rate of evaporation.

This work relates to drying of pig undergoing anaerobic digestate and a separation phase by centrifugation. Treated effluent has a solids content of 2.3%. In this context, an inclined stainless steel plate 2 m long, 1 m wide, and inclined by 30° has been put in place. The device is without a glass cover, and tests are carried in laboratory using a solar simulator in which power is 6000 W. This device is designed to be placed on barns roofs.

This study is divided into two parts. In the first part, evaporation tests were conducted by varying the inlet temperature of effluent. The second part will focus on comparison between experimental and calculated results by solving equations of heat and mass balances on plate and film.

**Nomenclature**

| | |
|---|---|
| $C_p$ | Heat capacity (J/kg.°C) |
| $e$ | Thickness (mm) |
| $h$ | Convection coefficient (W/m$^2$.°C) |
| $I$ | Radiated flux (W/m$^2$) |
| $L$ | Plate length (m) |
| $L_v$ | Latent heat of vaporization (J/kg) |
| $m$ | Flow (m$^3$/s) |
| Pr | Prandtl number |
| $S$ | Area (m$^2$) |
| $T$ | Temperature (°C) |
| $X$ | Horizontal axis (m) |
| $Y$ | Vertical axis (m) |
| *Greek letters* | |
| $\alpha$ | Absorptivity |
| $\mu$ | Viscosity (Pa.s) |
| $\varepsilon$ | Emissivity |
| $\upsilon$ | Kinematic viscosity (m$^2$/s) |
| $\zeta$ | Transmissivity |
| $\sigma$ | Boltzmann constant |
| $\lambda$ | Thermal conductivity (W/m.°C) |
| *Superscripts* | |
| * | Par unit width |
| *Subscripts* | |
| ev | Evaporated |
| in | Initial |
| ext,out | Outside |
| int | Inside |
| f | Fluid |
| p | Plate |
| pair | Between plate and air |
| pf | Between plate and film |

## 2 Effluent Characteristics

A thermophysical characterization of the effluent is performed to determinate thermal conductivity "$\lambda$," heat capacity "$C_p$," and dynamic viscosity "$\mu$." It's the liquid phase of pig manure which has already undergone a methanation and a separation phase by centrifugation.

Analyzes were performed on three samples ($E_0$, $E_1$ and $E_2$) having different concentrations. The sample $E_0$ is liquid effluent having a concentration $C_0$ and a dry matter content of 2.3%. The sample $E_1$ was prepared by evaporation of $E_0$ so as to

**Table 1** Characteristics of samples to analyze

| Sample name | $E_0$ | $E_1$ | $E_2$ |
|---|---|---|---|
| Concentration | $C_0$ | $C_1 = 1.5C_0$ | $C_2 = 3C_0$ |
| Density (g/l) | 960 | 900 | 850 |

**Table 2** Thermal conductivity of samples

| Sample | $E_0$ | $E_1$ | $E_2$ | Water |
|---|---|---|---|---|
| $T = 30$ °C | 0.593 | 0.560 | 0.598 | 0598 |
| $T = 60$ °C | 0.700 | 0.805 | 0.713 | 0.651 |

lose one-third of its initial volume. As for $E_2$, evaporated volume is about two-thirds of volume of $E_0$. The characteristics of each sample are shown in Table 1.

The thermal conductivity measurements with a device called FP2C. This is a thermal conductivity meter which is based on hot wire method for measuring the overall thermal conductivity of a material from evolution of temperature measured by thermocouple placed near a resistive wire. The values of thermal conductivity $\lambda$ are expressed in W/m.K. We were able to determine thermal conductivities of samples for 30 and 60 ° C (Table 2).

Knowing that measurement accuracy is 5%, and by referring to Table 2, we see that thermal conductivity does not depend on the concentration of the samples but depends on its temperature. When temperature is about 30 °C, it is 0.584 W/m.K almost equal to that of water of the order of 0.598 W/m.K. The thermal conductivity is about $\lambda = 0.739$ W/m.K, while $\lambda_{water} = 0.651$ W/m.K, at 60 °C (Brau 2006).

Measurements of dynamic viscosity are made by using a rheometer DHR III having TA Instrument mark. Measurements are performed at atmospheric pressure for three temperatures (20, 45, and 70 °C). Each test was performed twice on different samples to assess the reproducibility.

Before starting measurements, sample is deposited on bottom plate and spread with a top plate. Excess product is removed with a spatula. The gap is then adjusted and temperature of sample conditioned to be measured with an accuracy of 0.5 °C.

Flowing curve of different samples is obtained using a measuring method based on a constant shear rate. The values of shear stress and viscosity are noted as soon as flow is established. Results are given with an accuracy of 10%, considering geometries imperfections and rheometer accuracy (Fig. 1).

The influence of temperature on viscosity of each sample is shown. If temperature increases, viscosity decreases for different shear rates. However, this influence is less depending on sample, well marked for $E_0$ and $E_1$ (especially between 20 and 45 °C), and less important for $E_2$. Viscosity of sample $E_0$ is the closest to that of water (Brau 2006).

As for the measures of the heat capacity, they are made with the DSC Mettler Toledo DSC1. This device uses the differential scanning calorimetry (DSC), which measures the change in enthalpy in sample using a standard sapphire.

This method uses the following experimental conditions:

- Temperature stabilizing at 20 °C for 5 min, heating from 20 to 70 °C (20 °C/min)
- Stabilization at 70 °C for 5 min
- Continuous wipe neutral gas (nitrogen) to 50 ml/min

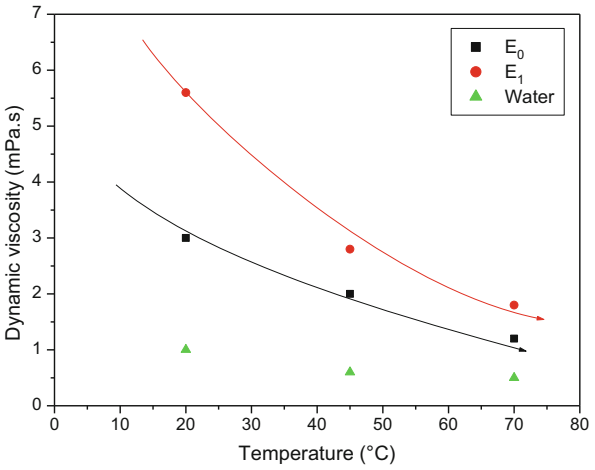


**Fig. 1** Graph of dynamic viscosity as function of temperature for shear rate of 100 $s^{-1}$

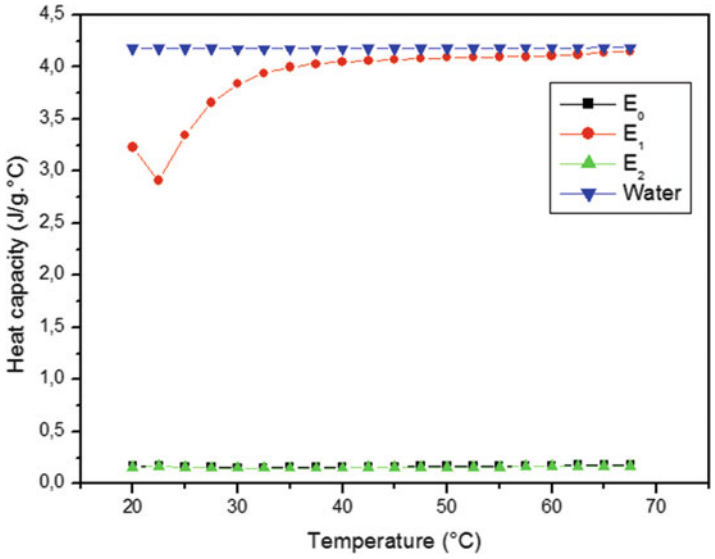


**Fig. 2** Heat capacity function of temperature for each sample

The analysis results show that for samples $E_0$ and $E_2$, heat capacity is constant over temperature range of 20–67.5 °C. It is an average of 0.166 J/g.°C for $E_0$ and 0.16 Jg.°C for $E_2$. For $E_1$, the heat capacity varies depending on the temperature. It is from 3.23 J/g.°C to $T = 20$ °C and decreases to 2.91 J/g.°C to 22.5 °C and gradually increasing. A slight increase is observed for temperatures between 30 and 67.5 °C; it is on average 4.08 J/g.°C. Results are shown in Fig. 2.

## 3 Experimental Facility

This process consists of flowing the aqueous liquid effluent on an inclined plate subject to solar flux. The purpose is to produce solid fertilizer from aqueous liquid waste, such as anaerobic digestate. The system should be inexpensive to purchase and consume as little energy as possible as it is for farmers who make liquid methane.

This device is an evaporator composed of a stainless steel plate with a tilt angle of 30°. This plate is 2 m long and 1 m wide. The liquid is injected from the top of the plate with an injection nozzle. Fluid flows along the plate and is recovered in a gutter (Fig. 3).

The steel plate isn't covered with glass wool. It is heated using a 6000 W solar simulator. Solar simulator is placed parallel to the evaporator at a distance of 2 m such that the flow will be focused on of the upper part of plate and there will be a flux density similar to that of the sun.

Thermocouples were fixed to the stainless steel plate, as shown in Fig. 4. The thermocouples are positioned into three rows of nine lines. The first line of thermocouples is approximately 20 cm from the top and 15 cm for the edge. Thermocouples are spaced at a distant of 20 cm. K-type thermocouples were used and had a margin of error of ±2.5 ° C.

Once steady state is achieved, the liquid was injected from the top of the plate using a pump that feeds the dispense manifold. The input flow measurement was performed by weighing the liquid before and after injection for a predetermined time before the start of the solar simulator.

The evaporated flow was measured when the simulator was powered and after stabilization of the temperature. The measurement was achieved by weighing the liquid at the output of the plate over a given time.

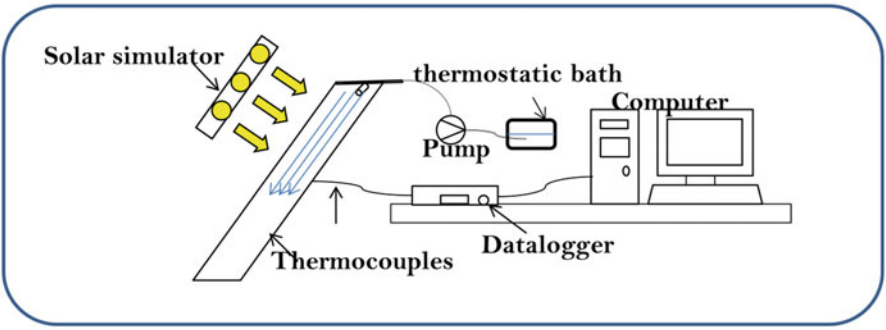


**Fig. 3** Experimental installation

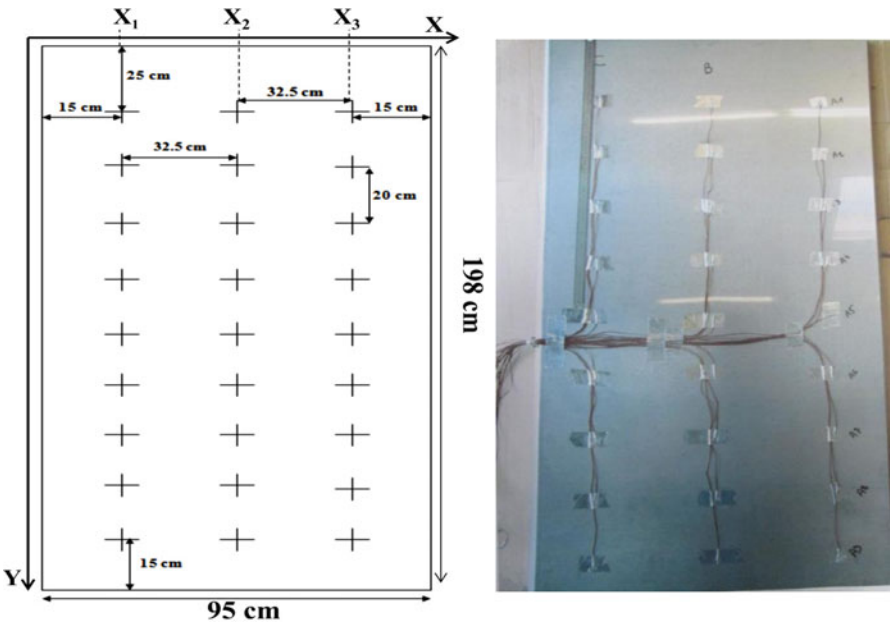


**Fig. 4** Layout of thermocouples on the plate

## 4 Numerical Scheme

Before circulating liquid film, the plate exposed to radiation simulator and its back is isolated (no heat loss). Based on the sum of the incoming flux equals the amount of outgoing flux, the heat balance on the plate can then be written:

$$\alpha_p I_0 - \varepsilon_p \sigma \left( T_p^4 - T_{air}^4 \right) - h_{ext,pa} \left( T_p - T_{air} \right) = 0 \tag{1}$$

The natural convection coefficient in steady state is a function of temperature of the plate and that of air (Chen et al. 1986; Huezt et al. 1981):

$$h_{ext,pa} = 0.225 \left( T_p - T_{air} \right)^{1/5} \tag{2}$$

Heat balance becomes:

$$\alpha_p I_0 - \varepsilon_p \sigma \left( T_p^4 - T_{air}^4 \right) - 0.225 \left( T_p - T_{air} \right)^{6/5 = 0} \tag{3}$$

Once plate temperature stabilized, the liquid is circulated (Fig. 5).

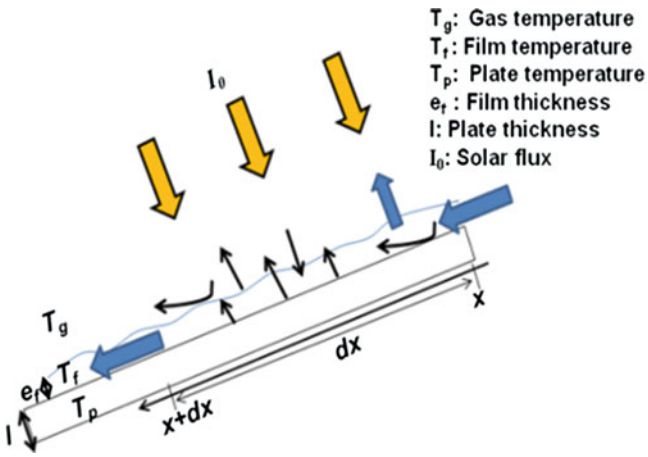


**Fig. 5** Balance on liquid film

Heat balance on film can be written:

$$\alpha_{\mathrm{p}}\tau_{\mathrm{f}}I_0 + \varepsilon_{\mathrm{p}}\alpha_{\mathrm{p}}\sigma T_{\mathrm{f}}^4 - \varepsilon_{\mathrm{p}}\sigma T_{\mathrm{p}}^4 - h_{\mathrm{int,pf}}\left(T_{\mathrm{p}} - T_{\mathrm{f}}\right) = 0 \tag{4}$$

The forced convection coefficient is a function of the thickness of the water film. In steady state, for an inclined plate of 30°, the forced convection coefficient between the effluent and the plate takes the following form:

$$h_{\mathrm{int,pf}} = \left(0.332.\frac{\lambda}{L}\mathrm{Pr}^{1/3}\sqrt{\frac{\dot{m_{\mathrm{in}}}}{\upsilon}}\right)\frac{1}{\sqrt{e_{\mathrm{f}}}} \tag{5}$$

As regards the liquid film, the mass balance is (Bouchekima et al. 2001):

$$\begin{aligned}&\dot{m}\,(x)C_{\mathrm{p}}\frac{T_{\mathrm{f}}(x)}{dx} + \alpha_{\mathrm{f}}I_0 + \alpha_{\mathrm{f}}\tau_{\mathrm{f}}\rho_{\mathrm{p}}I_0 + h_{\mathrm{int,pf}}\left(T_{\mathrm{p}}(x) - T_{\mathrm{f}}(x)\right)\\ &+\alpha_{\mathrm{p}}\varepsilon_{\mathrm{p}}\sigma T_{\mathrm{p}}^4 = \left(\dot{m}\,(x) - \dot{m}\,(x+dx)\right)Lv + h_{\mathrm{int,fair}}(T_{\mathrm{f}} - T_{\mathrm{air}})\\ &+\varepsilon_{\mathrm{f}}\sigma T_{\mathrm{f}}^4 + \dot{m}\,(x+dx)C_{\mathrm{p}}\frac{T_{\mathrm{f}}(x+dx)}{dx}\end{aligned} \tag{6}$$

where:

$$S_{\mathrm{p}} = dx.L \quad \text{and} \quad \dot{m_{\mathrm{ev}}} = \dot{m_{\mathrm{in}}} - \dot{m_{\mathrm{out}}} \tag{7}$$

The film thickness along the plate is variable and depends on the evaporated flow. Assuming the volume is constant, the film thickness is defined by:

$$e_{\mathrm{f}}(x) = e_{\mathrm{f}}(0).\frac{\dot{m}\,(x)}{m_{\mathrm{in}}} \tag{8}$$

The equations are solved using the programming language MATLAB. Solving equations is performed one by one as the number of equations is less than the number of unknowns. Once temperature along the plate is determined from Eq. (3), it is known and entered as data in (4). Knowing $T_p(0)$ and $T_f(0)$, we can determine the convection coefficient. Thus, Eq. (6) is solved at initial status. Using (8) the film thickness is known to state $x$ and did the same approach to solving (4) and (6).

## 5 Results and Discussions

The cartography of the flux on plate is shown in Fig. 6. We chose the same points as thermocouples (three columns of nine lines). The solar flux is measured by a pyranometer with accuracy ±4–10 μV/W/m$^2$.

The maximum flux is at $Y = 0.45$ m according to the different positions $X_1$, $X_2$, and $X_3$. It is 805 W/m$^2$ at $Y = 0.45$ m for position $X_2$. The minimum flux is 111 W/m$^2$ for $Y = 1.85$ m for position $X_1$. The mean flux along plate is approximately 424 W/m$^2$.

The shape of this curve can be explained by the position of simulator in which plate is exposed. Therefore, the flux is not distributed evenly; it is only the upper part of plate which is exposed to radiation. From point $Y = 1.45$ m, simulator just radiates; this partly explains the fall of the stream up to 116 W/m$^2$.

By solving Eq. (1), we were able to compare temperature of plate in different experimental and calculated positions. Results are shown in Fig. 7.

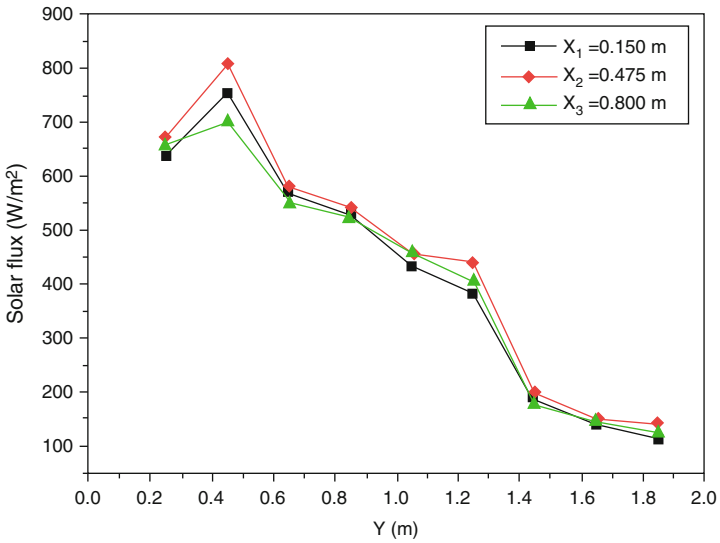


**Fig. 6** Cartography of the fluxes on the plate

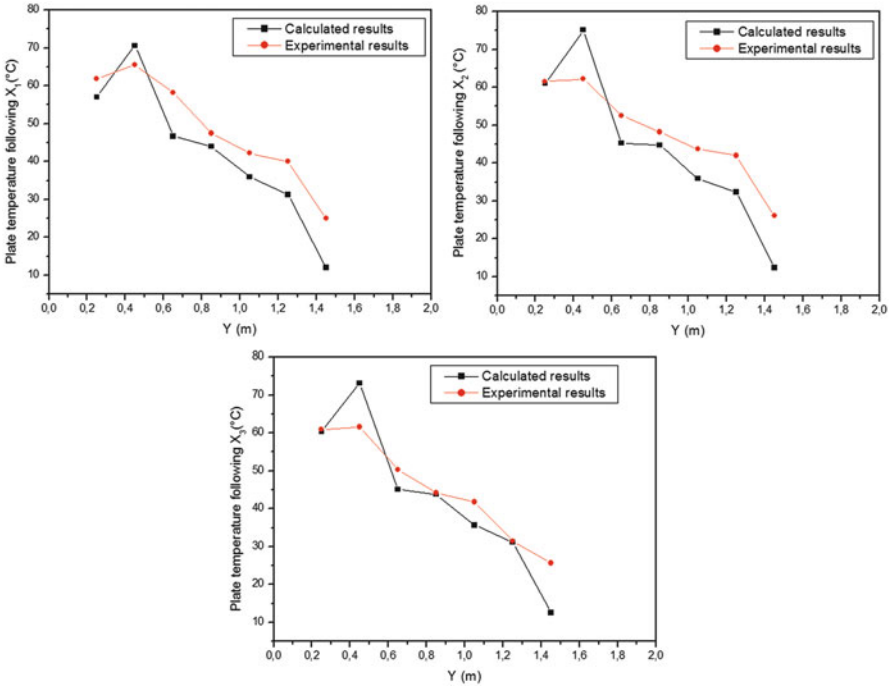


**Fig. 7** Evolution of plate temperature

At the colomn $X_1$, $X_2$, and $X_3$, plate temperature have the same shape. It is maximum at $Y = 0.45$ m and decreases along plate. This can be explained by the solar flux which is focused on the top plate when it reaches 805 W/m$^2$.

From Eq. (1), temperature of plate depends on radiation flux and temperature of the air. The flux is not uniformly distributed on plate, whose upper portion is only exposed to radiation. This explains the drop in temperature of plate from $Y = 1.45$ m. This curve has the same shape as the distribution curve of flux along plate. Then, temperature of plate is strongly dependent of radiated flux.

The slight variation of calculated and measured plate temperature may depend on several factors such as laboratory temperature and temperature of the air between plate and simulator.

The liquid flows over plate. By varying inlet temperature of effluent, the temperature of effluent on plate varies as shown in Fig. 8, according to Eq. (4).

Temperature of effluent increases on top of plate; when the maximum is reached at $Y = 0.45$ m, it starts to decrease until stable bottom of plate. When liquid inlet temperature is 40 °C, fluid reaches a maximum temperature of 69 °C at $Y = 0.45$ m and for $X_2 = 0.475$ m. Then its temperature decreases to 38 °C at $Y = 1.85$ m and for $X_2$.

In each case, film temperature is maximal for $X_2$. This can be explained by the distribution of flux, which is maximum at the top of plate. Moreover, from Eq. (4),

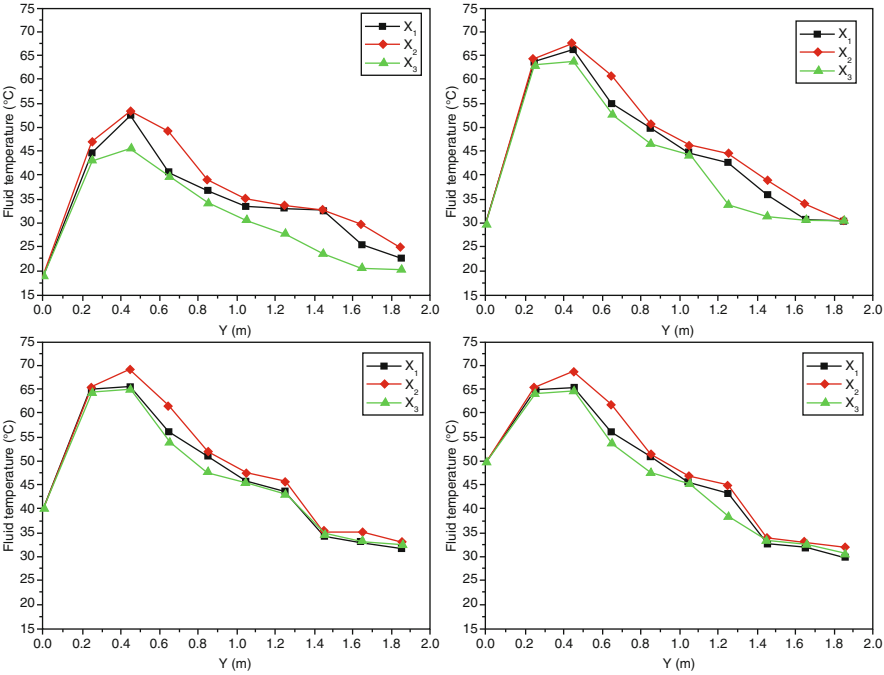


**Fig. 8** Film temperature along the plate

the variation in $T_p$ causes the variation of $T_f$. This implies that fluid temperature curve along plate has the same shape as that of plate. The fall of fluid temperature is due to the low temperature of plate that is not exposed to the rays of simulator.

On the top, temperature of plate is higher than of fluid. Fluid is heated by plate. Its temperature increases and is close to that of plate. The bottom of plate with fluid reaches a higher temperature and cools this part of plate.

We compared the inlet and outlet liquid temperatures; results are shown in Fig. 9:

When the liquid is preheated at 20 and 30 °C, its outlet temperature is higher than of input. It is, respectively, 24 and 34 °C experimentally and 23 and 31 °C calculated. Hot liquid having a temperature around 35 °C is cooled on the bottom of plate. The difference between plate and fluid temperature is low. If liquid is preheated at 40 and 50 °C, the difference of temperature between plate and fluid is large, hence temperature drop of the latter in outlet. As for maximum difference between measured and calculated results, it is 10%.

Evaporated local flow is maximum when liquid temperature is high. It gradually decreases. It is low in the bottom of plate because fluid temperature is low (Fig. 10).

Experimentally, we measured the total throughput evaporated. Theoretically, it is determined by integrating the local flow evaporated. We obtained results presented in Fig. 11.

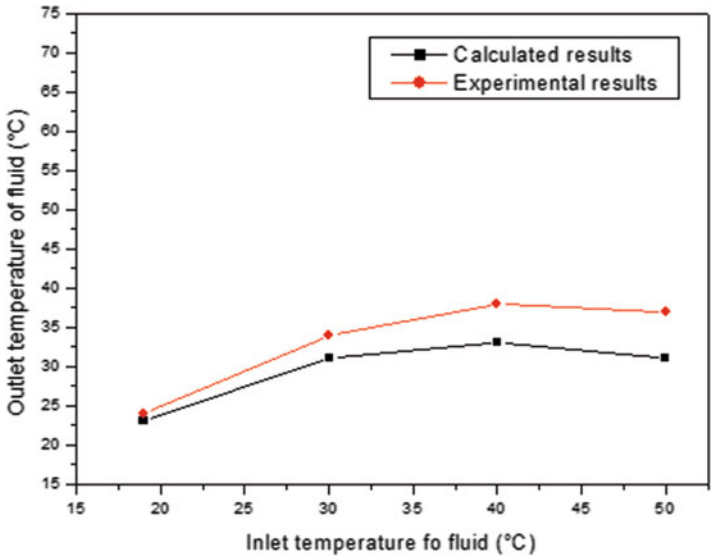


**Fig. 9** Outlet temperatures of fluid

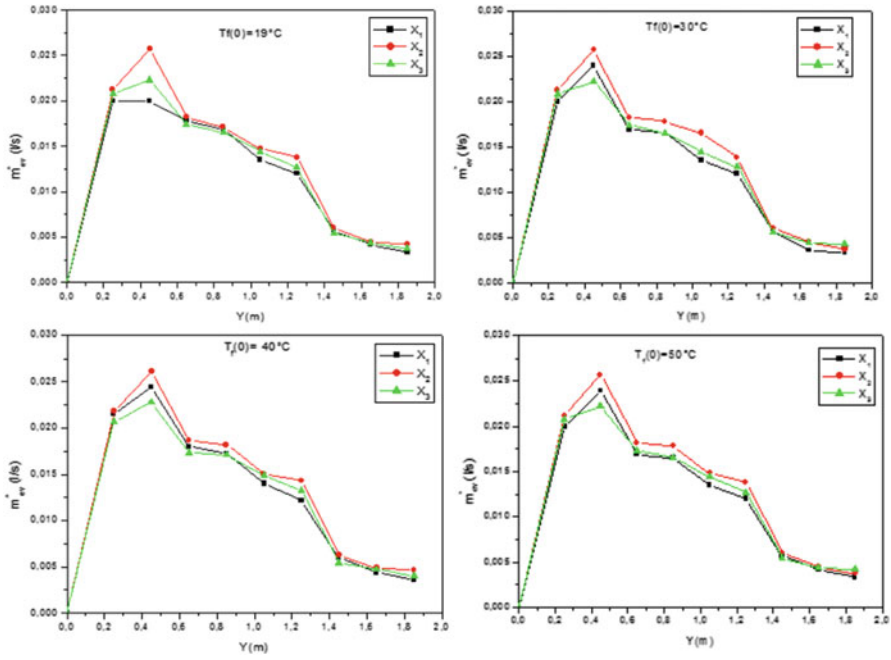


**Fig. 10** Variation of local evaporated flow along plate

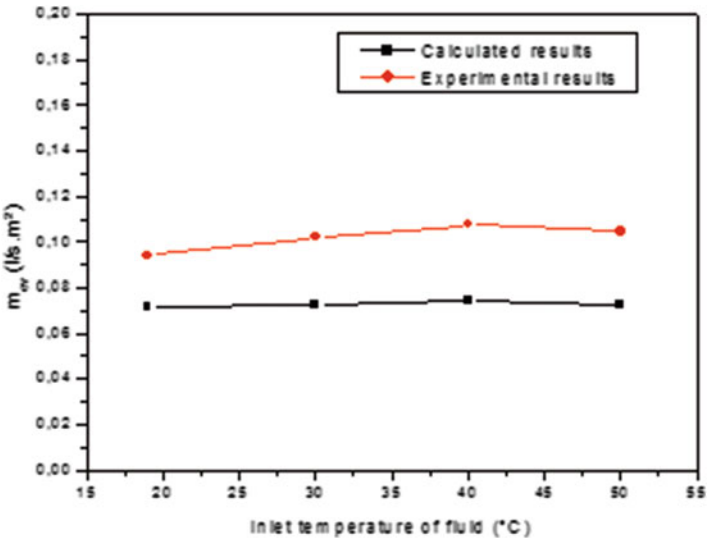


**Fig. 11** Comparison between calculated and experimental evaporated flow

We find that when liquid is preheated at temperatures between 19 and 40 °C, the total flow increases evaporated if inlet temperature is increasing. From an inlet temperature of 50 °C, liquid is warmer than the plate and vacates its heat. This explains the decrease in total flow evaporated at this temperature. The maximum difference between measured and calculated results is 10%.

The film thickness is variable; it decreases along plate until it stabilizes when evaporated flow becomes weak. The curves of Fig. 12 are the results of solving Eq. (8).

Film thickness is the lowest for $X_2$ for each case where evaporated flow is maximum. More evaporated flow increases; film thickness is low and vice versa. The significant decrease of film thickness is due to the high evaporated flow. In bottom of plate, evaporated flow is low and film thickness is almost constant.

Volume concentration of effluent increases following $Y$. Flowing liquid evaporates and loses its water content. It becomes more concentrated. Note that initial volume concentration of liquid is 0.0229%. At its release, its maximum concentration reached 0.0274% (Fig. 13).

At the bottom of plate, liquid concentration stabilizes due to low evaporated flow. Volume concentration is maximum following $X_2$, evaporated maximum flow along this axis. The concentration of liquid at output is maximum when liquid is preheated to 40 °C. It reaches 0.0274 in output.

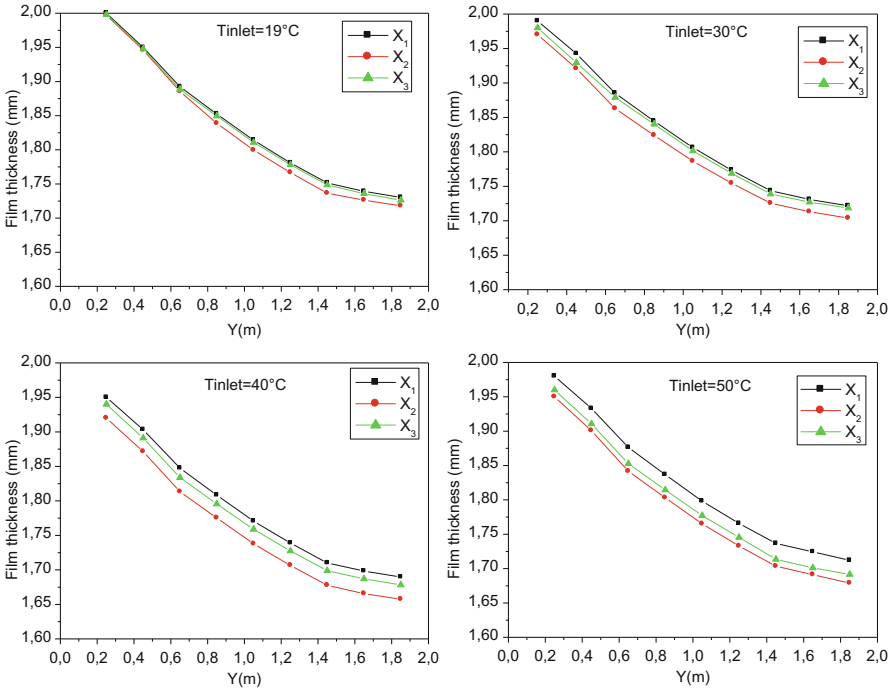


**Fig. 12** Variation of thickness film along plate

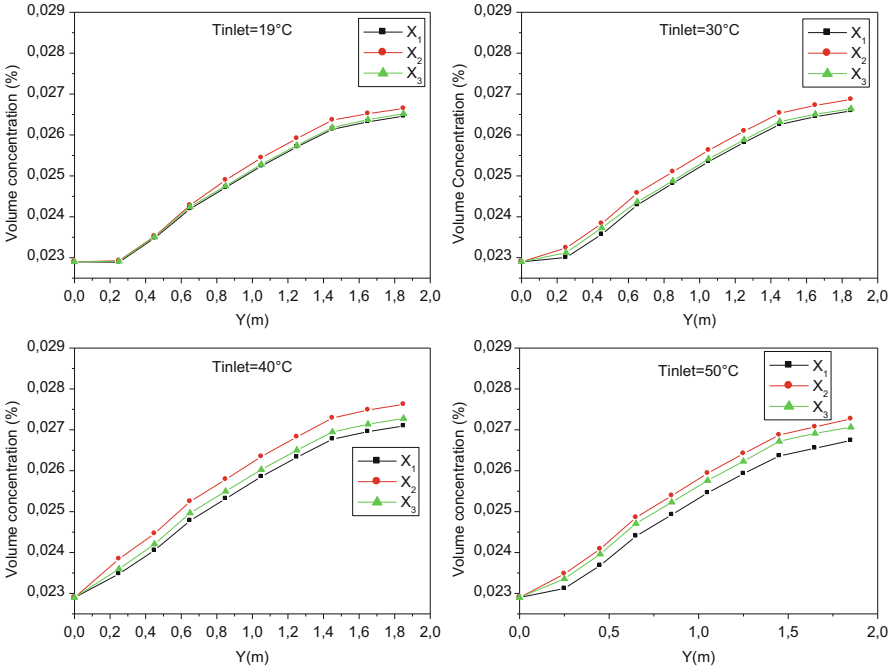


**Fig. 13** Variation of effluent concentration along plate

## 6 Conclusion

A study on evaporation of a pig digestate after centrifugation was established. The effluent having 2.3% of dry matter is flowing as film on a stainless steel plate inclined by 30°. A thermophysical characterization of three samples of different concentrations shows that heat capacity and viscosity depend on the concentration of liquid. However, thermal conductivity doesn't depend on liquid concentration but on its temperature.

A comparison between experimental and calculated results by determining heat and mass balance on plate and film was completed. The comparison between measured and experimental results doesn't exceed 7%. We found that since heating flow isn't constant over plate, temperature of plate depends on flux distribution. If it's maximum, then plate temperature is maximum and vice versa. Once film circulates, its temperature is affected by temperature of plate. Thereby evaporated flow is proportional to film temperature.

Evaporated flow is maximum on the central part of plate, where flux is maximum. The final concentration of product reached 0.0274%. Liquid has lost nearly 20% of its volume when the liquid is introduced at 40 °C. Therefore, when we preheat liquid between 19 and 40 °C, evaporated flow improves. So, liquid temperature becomes higher than that of plate. And, liquid transfers its heat to the plate that blocks evaporation phenomenon.

**Acknowledgments** This research is a part of a Ph. D study in National Engineering School of Monastir in Tunisia. It's supported by the Laboratory TEMPO of the University of Valenciennes and Hainaut-Cambresis.

## References

Bennamoun, L.: Solar drying of wastewater sludge: a review. Faculté des Sciences Exactes, Sciences Naturelles et de la Vie, Université Larbi BenM'hidi, Oum El Bouaghi, Algeria Article history (2011)

Bouchekima, B., Gros, B., Ouahes, R., Diboun, M.: Brackish water desalination with heat recovery. Desalination. **138**, 147–155 (2001)

Brau, J.: Support de cours de convection pour 3 GCU. Insa de Lyon, département de Génie Civil et Urbanisme (2006)

Chen, T.S., Tien, J.P., Armaly, B.F.: Natural convection on horizontal, inclined and vertical plates with variable surface temperature or heat flux. Int. J. Heat Mass Transf. **29**(10), 1465–1478 (1986)

Granier R, Texier C. Production du lisier de porc à l'engrais: quantité et qualité. Techni-porc, pp. 23–31 (1993)

Granier, A., Badeau, V., Breda, N.: Modélisation du bilan hydrique des peuplements forestiers. Revue Forestière Française, 1995, S, fascicule thématique "Modelisation de la croissance des arbres forestiers et de la qualité des bois" (1995)

Huetz-Aubert, J., Sacadura, F.: Mesure des émissivités et des réflectivités monochromatiques directionnelles des matériaux opaques. Revue Phys. Appl. **17**, 251–260 (1981)

Latimier, P., Gallard, F., Corlouër, A.: Actualisation des volumes et des quantités d'azote, de phosphore et de potasse rejetés dans le lisier par un élevage naisseur-engraisseur. Journées Rech. Porcine en France. **28**, 241–248 (1996)

Levasseur, P.: Composition et volume de lisier produit par le porc : Données bibliographiques. TECHNI. **21**(4), 16–19 (1998)

Lei, Z., Dezhen, C., Jinlong, X.: Sewage sludge solar drying practise and characteristics study. In: Proceedings of Power Engineering Conference, IEEE (2009)

Mani, A., Srinivasa Murthy, S.: Solar Evaporation Ponds for Tannery Effluent Treatment. A Technical Report. TALCO Ltd., Chennai (1993)

Mani, A., Srinivasa Murthy, S.: Analysis of an open type flat plate collector for tannery effluent treatment. Energy Convers. Manag. **35**(12), 1061–1071 (1994)

Salihoglu, N.K., Pinarli, V., Salihoglu, G.: Solar drying in sludge management in Turkey. Renew. Energy. **32**, 1661–1675 (2006)

Srithar, K., Mani, A.: Analysis of a single cover FRP flat plate collector for treating tannery effluent. Appl. Therm. Eng. **24**(5–6), 873–883 (2003)

Srithar, K., Mani, A.: Comparison between simulated and experimental performance of an open solar flat plate collector for treating tannery effluent. Int. Commun. Heat Mass Trans. **30**(4), 505–514 (2004)

Srithar, K., Mani, A.: Studies on solar flat plate collector evaporation systems for tannery effluent (soak liquor). J. Zhejiang Univ. Sci. A. **7**(11), 1870–1877 (2006)